Reflections on the Importance of Small Strain Non-Linearity in Soils

Andrew J. Whittle[1]
[1]*Department of Civil & Environmental Engineering, Massachusetts Institute of Technology, Cambridge, MA 02139, USA*
E-mail: ajwhittl@mit.edu

ABSTRACT: It is widely accepted today that most soils exhibit non-linear stress strain properties even at very small strain levels and that improved representation of these stiffness properties is needed to understand and interpret many practical problems involving soil-structure interactions. Much of this understanding relates to research carried out at Imperial College led by John Burland and his colleagues during the 1980's. This work included the development of devices for routine measurements of local strains in laboratory element tests (Burland & Symes, 1982; Jardine et al. 1984), documentation of small strain stiffness properties for a range of reconstituted and natural soils (Jardine et al. 1984), and representation of these nonlinear stiffness properties in finite element simulations involving a range of soil-structure interactions (Jardine et al. 1986). This information was then synthesized in Burland's seminal Bjerrum Lecture '*Small is beautiful*' (Burland, 1989) and linked to the performance of foundations, excavations and tunnels. This paper reviews the importance of small strain non-linearity from the perspectives of i) advancing knowledge of soil behavior, ii) development of more reliable constitutive models, and iii) evaluating impacts in the computed performance for practical geotechnical problems.

KEYWORDS: Soil stiffness properties, Laboratory tests, FE analyses, Constitutive models, Foundations, Excavations, Tunnels

1. INTRODUCTION

I was a final year undergraduate student when John Burland returned to academia as Professor of Soil Mechanics at Imperial College (1980). It was a time of palpable excitement, change was in the air (the first IBM PC appeared!) and Burland was the new face of soil mechanics, bringing his pioneering work on soil modelling at Cambridge and field experience at BRE. He was supported by an incredibly vibrant and energetic group of researchers who assisted with our labs and design projects (including 4 future Rankine lecturers). Over the next few years, the research done by Burland and his colleagues re-shaped soil mechanics, largely through improved laboratory measurements, insights on the small strain, non-linear stiffness properties of soils and their role in understanding soil-structure interactions.

Burland (1989) begins his 1989 Bjerrum lecture by recalling some experiences where the stiffness of soils back-figured from field measurements (shallow foundations on weathered chalk and stiff clay) were much higher than those measured in conventional laboratory triaxial shear tests. The prevailing wisdom in the 1970s was to attribute the low stiffness values to sample disturbance in lab tests. This situation changed through measurements of local strains on test specimens. Symes and Burland (1982) describe the design of electrolyte liquid level sensors (electrolevel transducers), that were previously used by BRE (to measure ground tilt around piles) for accurate measurements of local axial strains on triaxial test specimens. Using a refined geometric design of these sensors, Jardine et al. (1984) reported data from suites of undrained shear tests on a range of clays from remoulded and reconstituted marine clay, to intact very stiff clays and pluviated sands. While conventional end-end strain measurements become unreliable at axial strain levels, $\varepsilon_a < 0.05$ - 0.1%), the electrolevel gauges were able to measure to strains $\varepsilon_a \sim$ 0.001% and the Authors report secant stiffness (E_u) values over the range ε_a = 0.005 – 10%. The data show increasing secant stiffness with decreasing levels of log(ε_a) . Typical secant stiffness values at ε_a = 0.01 are higher than those at 0.1% by a factor of 2 – 5 (the Authors report $E_{u(0.1)}/E_{(0.01)}$ = 0.18 – 0.52 over all materials and stress histories).

Jardine et al. (1986) investigated how the measured non-linear stiffness properties could influence predictions of soil-structure interaction. They fitted a non-linear stiffness function, $E_u/C_u(\varepsilon_a)$, to the measured data and conducted a series of undrained finite element analyses of relatively simple boundary value problems (C_u is the undrained strength represented by a Tresca criterion). The analyses illustrate the importance of small-strain non-linearity on the distributions of ground movements around foundations and propped excavations. The Authors also compare 'apparent values of the normalized secant stiffness' (E_u^A/C_u) interpreted directly from the numerical simulations as functions of the load factor (LF = 1/FS, where FS is the factor safety against undrained failure). These results show large differences in E_u^A/C_u at a selected LF, highlighting the confusion arising in the back-analyses of apparent soil moduli from different classes of boundary value problem.

The timing of these contributions was significant. They coincided with the emergence of computer control and automation in geotechnical lab testing (e.g., Sheahan et al. 1990) and pre-date commercial finite element codes. Small strain non-linearity became a hot research topic – leading to a series of *International Symposia on Deformation Properties of Geomaterials* (the first in Sapporo in 1994 led to the creation of a new ISSMGE committee on lab testing; TC101).

This paper reviews the importance of small strain non-linearity from the perspectives of i) advancing knowledge of soil behavior, ii) development of more reliable constitutive models, and iii) evaluating impacts in the computed performance for practical geotechnical problems.

2. ADVANCING KNOWLEDGE OF SOIL BEHAVIOR

The initial measurements of small strain non-linearity (Jardine et al. 1984) can be viewed as a first step in bridging the gap between static and dynamic measurements of soil stiffness. Refinements in the design of local strain measurements (using LDTs, Goto et al. 1991; and LVDT systems; Cuccovillo & Coop, 1997; Santagata, 1998) have enabled static measurements of stiffness at strain levels, $\varepsilon_a = 10^{-4}\%$ - $10^{-3}\%$, where most soils reach a linear elastic limit (constant modulus; Tatsuoka et al. 1994, Santagata et al. 2007).

The soil dynamics community have long focused on the small strain stiffness properties that control the propagation of elastic body and surface waves (particularly the maximum/elastic shear modulus, G_0). Similarly, in earthquake engineering, the degradation in stiffness and hysteretic damping (with the level of shear strain, γ) are essential inputs in 1-D site response analyses (associated with vertically-propagating, horizontally-polarized shear waves, SH). These properties have typically been measured using laboratory resonant column devices that impose cyclic torsional shear on cylindrical test specimens (Drnevich et al. 1978), within a strain range where there is almost no irrecoverable behavior (typically, $\gamma \leq 0.03\%$; Clayton, 2011).

Figure 1 illustrates the configuration of an advanced triaxial test that includes local measurements of axial and radial strains, together with pairs of piezoelectric transducers (piezoceramic bender

elements) that measure local elastic shear wave velocity, v_s ($G_0 = \rho v_s^2$; this can be measured in the vertical or horizontal planes depending on transducer location and wave polarization). While the measurement principle is clearly defined there are significant practical issues in the accurate timing of wave travel (Clayton, 2011).

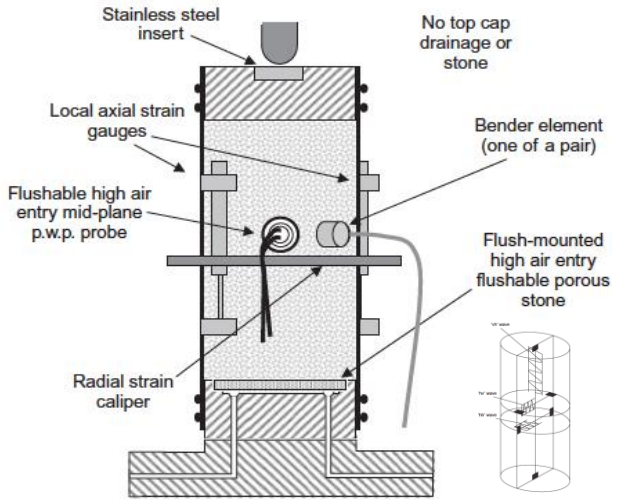

Figure 1 Advanced triaxial test set-up (after Clayton, 2011)

There appears to be a consensus that for a wide range of geomaterials the stress-strain behaviour is linear and elastic at strain levels less than ~ 0.001%, and that this behaviour is independent of strain rate (discrepancies between laboratory and field tests may still occur due to sampling disturbance etc.; Tatsuoka and Shibuya, 1992). Hence, bender elements can in principle provide either independent validation of G_0 measured by local strain systems (LVDT etc.) and/or provide additional data on anisotropy of elastic parameters (G_{vh}, G_{hh}, G_{hv}; Figure 1).

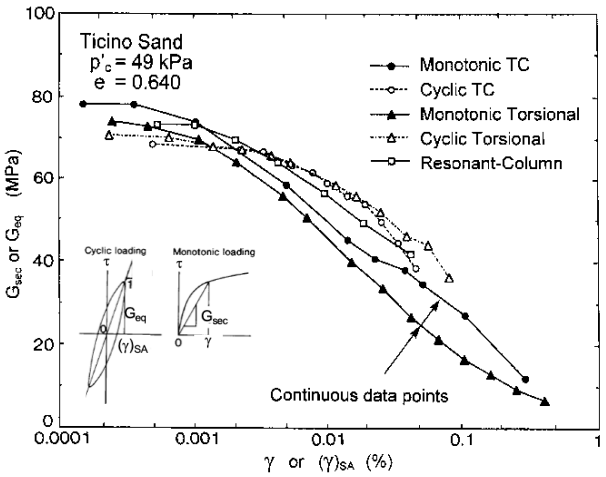

Figure 2 Comparison of secant shear moduli for isotropically-consolidated Ticino sand measured in static and dynamic laboratory shear tests (γ_{SA} – single amplitude shear strain from cyclic tests)

Figure 2 compares the degradation in the secant shear modulus measured in drained static monotonic and cyclic shear tests (in triaxial compression and torsional shear modes) with data from resonant column tests; for specimens of isotropically-consolidated, dense Ticino sand. Differences between the two modes of shearing can reflect inherent anisotropic stiffness properties, while comparisons of monotonic and cyclic shear reflect differences in strain rate. The data show reasonable convergence at shear strains, $\gamma \leq 10^{-3}$% (G_0 = 75±4 MPa), but there is higher degradation of stiffness in the monotonic vs cyclic tests (G_{sec} vs G_{eq}; Figure 2) for γ = 0.002 - 0.02%, suggesting significant rate effects. The cyclic shear data are in better agreement with RC data over this strain range. Collectively, these data suggest that shear strain rates do affect the small-strain non-linear stiffness properties of sands.

Figure 3 shows details of the stress-strain behaviour in undrained triaxial compression of K_0-normally consolidated, resedimented Boston Blue Clay (RBBC) sheared statically at strain rates, $\dot{\varepsilon}_a$ = 0.1 – 4.0%/hr. These data also show convergence to a unique small strain stiffness for $\varepsilon_a \leq 0.002$% (Figure 3), but there is a notable impact of strain rate on the degradation of stiffness $\varepsilon_a > 0.01$% (i.e., at strain levels where there are negligible shear-induced pore pressures; Santagata et al. 2007).

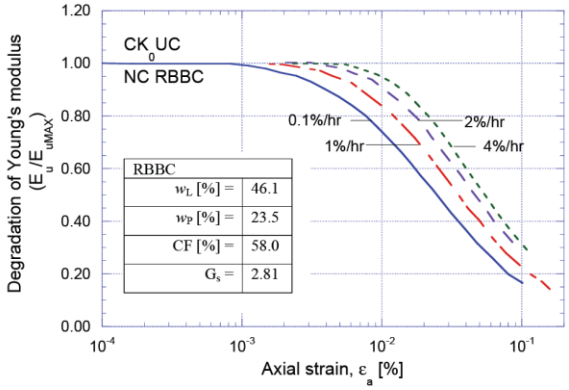

Figure 3 Effect of strain rate on small strain stiffness of K_0-normally consolidated re-sedimented Boston Blue Clay (after Santagata,1998)

There is a growing database of anisotropic soil stiffness properties at very small strain levels. As expected, results for reconstituted sands (e.g. Hoque and Tatsuoka, 1998; Bellotti et al. 1996) show modest effects of anisotropy (e.g., E'_h/E'_v = 1.0±0.2). Kim and Finno (2014) report similar ratios measured in triaxial test specimens from block samples of three lightly overconsolidated Chicago clays (G_{hh}/G_{hv} or G_{hh}/G_{vh} = 1.1 – 1.2), consistent with field cross-hole tests.

Much more significant elastic anisotropy has been measured in highly overconsolidated clays such as London Clay. Gasparre et al. (2007) present a unique study that measures anisotropic stiffness properties of intact London Clay (block samples from Heathrow T5 site) that combines elastic wave propagation and local strain data (in drained stress probe experiments) using triaxial and Hollow Cylinder test devices.

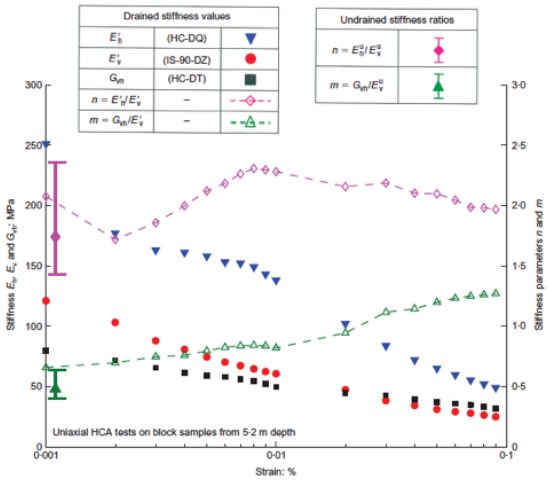

Figure 4 Degradation of anisotropic stiffness properties of intact London Clay (after Gasparre et al. 2007; Zymnis et al. 2013)

Bender element data show that London clay exhibits cross-anisotropic stiffness properties at very small strain levels. Figure 4 summarizes the degradation of three stiffness components (E'_v, E'_h, G_{vh}) vs strain level (up to 0.1%). The anisotropic stiffness ratio, n (= E'_h/E'_v) is largely unaffected by strain level (n = 2.0±0.3); while m (=

G_{vh}/E'_v) increases from 0.7 – 1.2. As far as I am aware, these are the first experiments that show small-strain non-linearity in directional stiffness properties.

The data show the importance of inherent anisotropy in elastic stiffness properties, which are related to the microstructural arrangement of particles. Most authors report linear elastic stiffness properties that are functions of the confining pressure and void ratio:

$$G_{max} = Af(e)(p'/p_a)^n \quad (1)$$

where p_a is the atmospheric pressure, A, n are constants (typically, n = 0.5±0.1; Mitchell and Soga, 2005).

There is also an increasing database of direct measurements of elastic properties from statistical interpretation of nanoindentation experiments which provide more direct information on the relationship between elastic properties ($Af(e)$ in Eq. 1) the particle packing and fabric (e.g., Bobko, 2008; Ortega et al. 2008).

Small strain non-linearity appears to be a general characteristic of all unbonded geomaterials (sands-clays-rocks). There is now a wealth of data showing continuous degradation of stiffness once strains exceed a threshold value (the threshold varies with soil type and level of effective confining stress but is typically in the range ~10^{-3}-10^{-2}%). Jardine (1985) reports the limit of linear elasticity as a locus around the current stress state (e.g., Y1 in Figure 5 corresponds to the linear limit for a threshold strain, ε_a = 0.01%).

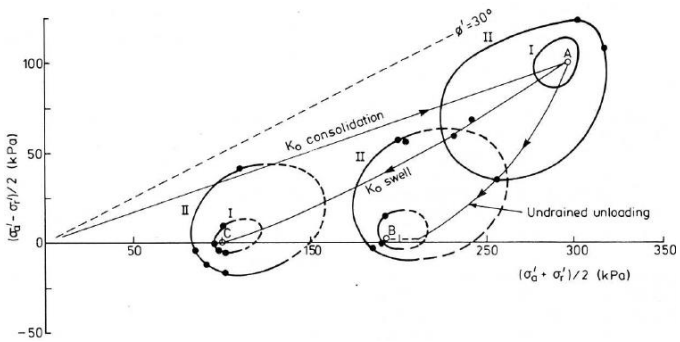

Figure 5 Threshold strain ('yield') surfaces Y1 and Y2 derived from local triaxial strain measurements for a reconstituted low plasticity clay (Burland, 1989; after Jardine, 1985)

A second locus (Y2; ε_a = 0.1%) defines the region where there is significant degradation in the secant stiffness. Burland (1989) indicates that there is little shear-induced pore pressure in the undrained effective stress paths (between Y1 and Y2) but asserts that strains are 'plastic and exhibit creep'. These observations are consistent with observation of energy dissipation (hysteretic damping), accumulation of shear-induced pore pressures (in undrained shearing), and or permanent deformations in cyclic loading over this strain range (e.g., Shibuya et al. 1995). Jardine et al. (2001) refer to Y2 as a volumetric strain threshold, where plastic deformations begin to impact volume changes in the pore space.

The origins of non-linear, inelastic deformations in the region Y1 – Y2 are not well defined but must relate to processes occurring at the particle (or particle contact) level. Jiang and Liu (2009) suggest a sub-division between macro-level entropy (associated with average particle movements) and particle level entropy production (due to changes in surface forces, irregular inter-particle movements, rolling/sliding at contacts, particle collisions etc.). This concept has been generalized by Kamrin and Bouchbinder (2014) who sub-divide the internal energy between configurational and vibrational degrees of freedom that fall out of equilibrium when acted upon by external agents (e.g., mechanical forces) that can be described macroscopically using viscoplasticity.

3. SOIL MODELING

It is interesting to recall the state of soil modelling contemporaneous with research on small strain non-linear stiffness (early 1980's). Incremental (work-hardening) plasticity was already established as a generalized framework, building on the success of critical state soil models such as Modified Cam Clay (MCC; Roscoe and Burland, 1968). Following the work of Iwan (1967) and Prévost (1977), Mroz et al. (1978, 1979) developed complex effective stress, multi-yield surface, kinematic hardening models. While these achieved some success in simulating the accumulation of plastic strains in cyclic loading, they notably lacked capabilities to describe small-strain non-linearity and hysteretic energy dissipation. Indeed, for practical applications, the most widely used formulations were either linearly elastic-plastic models (with Mohr-Coulomb [MC] yield, used in the first generation of commercial FE codes for geotechnical analyses such as Plaxis, 1993; Table 1) or density hardening models such as MCC. In either case, the stress-strain behaviour for all states below the state boundary surface was characterized by linear elasticity (or the non-linear elastic wall of MCC). Roscoe and Burland (1968) appreciated this limitation and proposed a second yield surface to describe plastic shear strains for overconsolidated clays.

Table 1 Family of elasto-plastic, effective stress soil models in Plaxis (note YS – yield surface orientation)

Model	Deformation: 1-D Comp.	Deformation: Shearing	Deformation: Non-Lin.	Shear Strength	Anisotropy	In Situ State	Basic Params
Mohr-Coulomb (MC; 'ancient')		E', ν'	–	c', φ', [ψ] OR s_u	–	K_0	3-5
Modified Cam Clay (MCC; Burland, 1968)	λ, κ	ν'		M(φ')	–	K_0, e_0, OCR	4
Hardening Soil (HS; Schanz (1998)	E_{oed}, E_{ur}	E_{50}, m		c', φ', [ψ]	–	K_0, OCR	6-7
HSS (Benz, 2006)	E_{oed}, E_{ur}	E_{50}, m	E_0, $\gamma_{0.7}$	c', φ', [ψ]	–	K_0, OCR	8-9
MIT-E3 (Whittle, 1987)	λ, κ_0, h	K_{ONC}, ν'	C, n, ω	φ'_{TC}, φ'_{TE}	c, s_t, ψ	K_0, e_0, OCR, YS	14
MIT-S1 (Pestana, 1994)	ρ_c, C_b, h	K_{ONC},μ'_0	D, r, ω, ω_s	φ'_{CS}	φ'_m, m, ψ	K_0, e_0, OCR, YS	13

The only model that was widely used to represent non-linear soil stiffness properties was the pseudo-elastic, hyperbolic model (DC; Duncan & Chang, 1970) which was incorporated in early finite element programs (together with the MC failure criterion). The DC model uses a hyperbolic function to represent stress-strain properties in shearing (using a single stress-dependent stiffness parameter that is a function of the confining pressure), a second stiffness parameter represents linear elastic behaviour in unloading and reloading (both parameters are power-law functions of the confining pressure). The original formulation was severely limited by the lack of a general loading criterion.

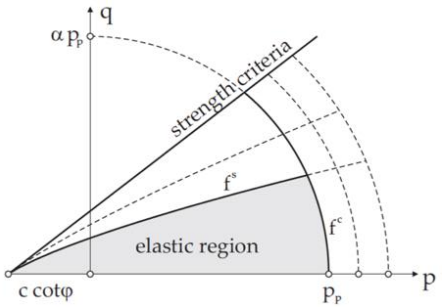

Figure 6 Framework of HS model using isotropic shear hardening to simulate nonlinear shear stiffness (Schanz et al. 2000)

Schanz et al. (2000) remedied this limitation by embedded the hyperbolic relations within a classical plasticity framework through a an isotropically yield function (f^s, Figure 6) defined in terms of the stress ratio ($\eta = q/p'$), and a flow rule based on Rowe's stress-dilatancy (Rowe, 1962). By including density hardening with a separate yield surface cap (f^c), the resulting Hardening Soil (HS) formulation is able to capture many aspects of clay and sand behaviour with a relatively small number of input parameters and state variables (Table 1). Indeed, the HS formulation skilfully hides the abstract modelling concepts from the user. However, HS does have a number of limitations: i) it does not include critical state conditions (for large strain shearing); ii) separate calibrations of input parameters are needed for each sand density/void ratio; and iii) the

hyperbolic equation is not able to match closely the small-strain non-linear stiffness properties.

Model predictions of small strain non-linearity were greatly improved through the incorporation of a small strain 'overlay model', where elastic modulus degradation is characterized by a paraelastic relation (i.e., the secant stiffness is related to recent strain history; after Hueckel and Nova, 1979) that is embedded within the framework of the HS model. Table 1 shows that the resulting HSS model include two new parameters (elastic stiffness E_0 [G_0] and a threshold strain, $\gamma_{0.7,}$ where G_{sec}/G_0 = 0.722) to represent the small strain stiffness.

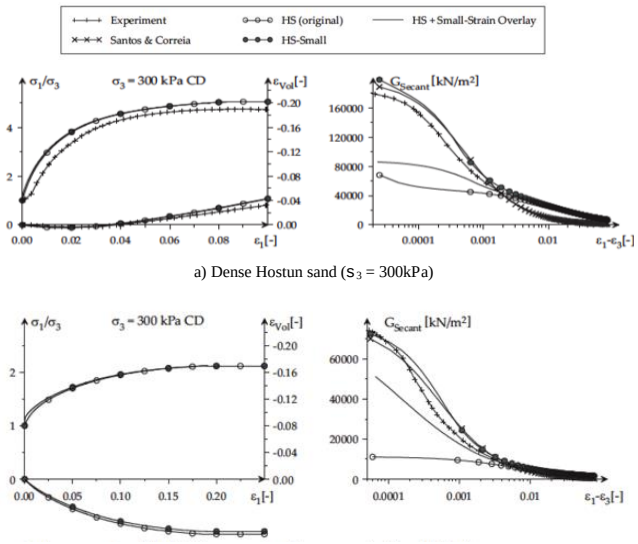

a) Dense Hostun sand (s_3 = 300kPa)

b) Kaolin (s_3 = 300kPa)

Figure 7 Comparison of computed and measured stress-strain and secant stiffness properties for dense sand and normally consolidated clay (after Benz, 2007)

Figure 7 shows that the HS and HSS (HS-Small) are effectively indistinguishable in their representation of the overall stress-strain properties, while HSS is able to represent the non-linear secant stiffness properties at small strains (in the range, $\gamma = [\varepsilon_1\text{-}\varepsilon_3]$ = 0.01 - 0.5%).

Small strain non-linearity was an integral feature of generalized effective stress soil models developed at MIT (Whittle, 1987; Pestana, 1994; Yuan, 2016). These models are based on a conceptual framework comprising three key components, as illustrated (for drained hydrostatic compression of clay) in Figure 8:

1. Plastic strains dominate the behaviour of normally consolidated clays (compression along VCL), inherent anisotropic properties are controlled by the orientation of the yield surface, while evolving anisotropy is characterized by kinematic hardening of the surface.
2. Elastic stiffness properties are revealed immediately at load reversal states (point A). Degradation of stiffness occurs during unloading but is largely path independent. Hysteretic behaviour (A-B-A; Figure 8a) is characterized by paraelastic functions related to the recent strain history (since the reversal state).
3. Plastic strains can accumulate during reloading as the stress state approaches the bounding surface of the normally consolidated clay (B-C Figure 8b). These strains are simulated using the framework of bounding surface plasticity (Dafalias and Herrmann, 1982).

The models use a single yield function/bounding surface and assume isotropic elastic properties at very small strains (i.e., anisotropy only develops due to plastic strains). The model framework is conceptually very similar to the empirical framework proposed by Jardine (1985) but does not explicitly include threshold stress surfaces (Y1, Y2; Figure 5).

The MIT-S1 formulation (Pestana, 1994; Pestana and Whittle, 1999) includes void ratio as a separate state variable in order to capture transitions from compressive to dilative properties using a single set of model input parameters.

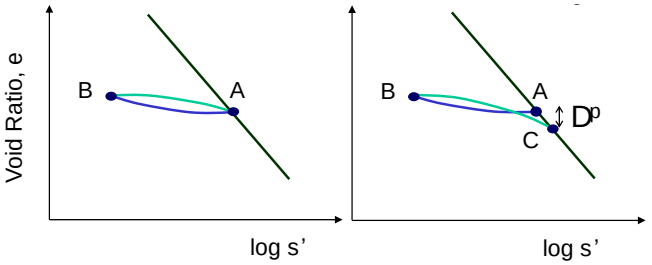

Figure 8 Conceptual framework of MIT-E3 soil model (Whittle, 1987; Whittle and Kavvadas, 1994)

Table 1 compares the elements of the MIT-E3 and MIT-S1 with other rate-independent elasto-plastic constitutive models available in the commercial FE code Plaxis. The HSS and MIT soil models share a similar approach to small strain non-linearity (para-elastic functions). This approach is similar to the concept to inter-granular strain introduced in hypo-plasticity by Niemunis and Herle (1997). The MIT models introduce additional parameters and state variables to represent (inherent and evolving) anisotropic properties through bounding surface behaviour. Kinematic hardening laws are used by many other constitutive formulations, especially those used to represent the cyclic response of soils (Wichtmann et al. 2019).

Assimaki et al. (2000) derived simplified form of the stiffness degradation and hysteretic damping functions (from the generalized MIT-S1 equations) for investigating 1-D site amplification in deep soil layers. Figure 9 shows that the paraelastic equations used by MIT-S1 achieve very good agreement with experimental measurements from (torsional shear) resonant column tests on dense sand over a wide range of confining pressures. The model simulates variations in the range of linear elastic strains without explicitly specifying a threshold condition (Y1).

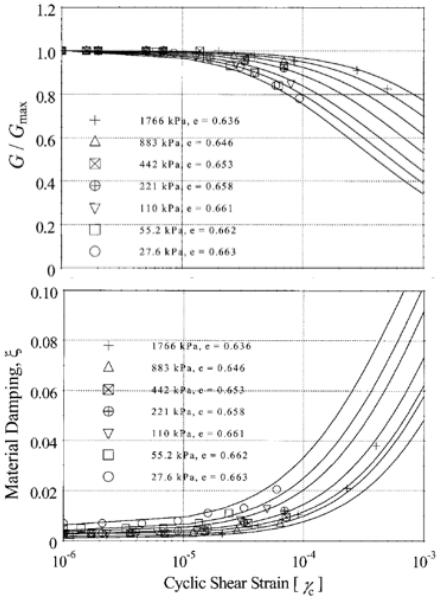

Figure 9 Comparison of MIT-S1 paraelastic (no plastic strain) modulus reduction and hysteretic damping with torsional shear RC data for a dense sand (Assimaki et al. 2000)

Elasto-plastic soil models are very widely used within geotechnical engineering, but do not represent the strain-rate dependence of modulus degradation as reported by Jardine et al. (1986). Figures 10a and 10b compare the effects of step changes in strain rate on the behavior of dense Hostun sand and reconstituted normally consolidated London clay. Both materials show an instantaneous response to the change in strain rate, but this effect appears to be transient for the sand (i.e., the response converges back

to a unique 'steady state' shear response). In contrast, step changes in strain rate for London clay appears to cause a shift in the steady state response (for each strain rate).

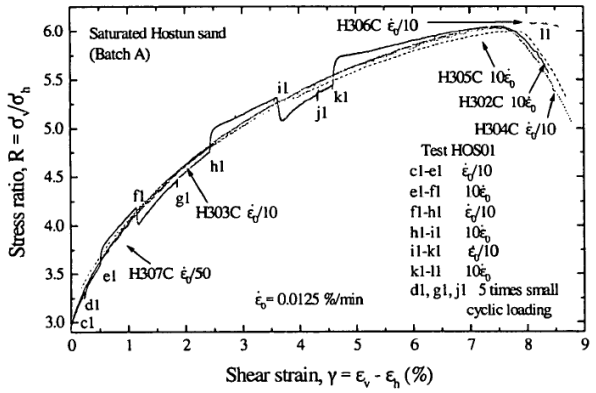

a) Dense Hostun sand (Di Benedetto et al. 2002)

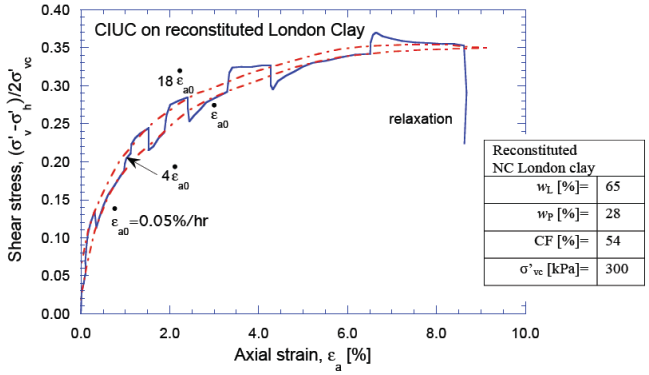

b) Undrained shear, reconstituted NC London clay (Sorensen, 2007)

Figure 10 Effect of step changes in shear strain rate on stress-strain response

Yuan and Whittle (2020a,b) have recently developed a generalized viscoplastic flow rule that can capture both types of behaviour within a generalized model of clay behaviour, MIT-SR:

$$\dot{\varepsilon}^{vp} = R_a \left(\frac{\sigma'_v}{\sigma'_{pe}} \right) \qquad (2)$$

where σ'_{pe} is the equivalent pressure, and R_a [1/time] is a state variable corresponding to an internal strain rate that is activated at the microscale due to the stimulation of historical straining (this is equivalent to the concept of granular temperature in non-equilibrium thermodynamics; Smith, 2001). By defining an evolution law for R_a (that includes activation, decay and steady state conditions) the MIT-SR model can represent the response of sands (Figure 10a previously represented by the TESRA model; Di Benedetto et al. 2002) or the isochrone-type behaviour observed for clay (Figure 10b).

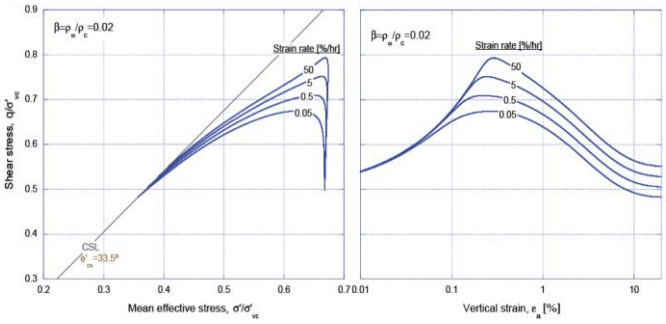

Figure 11 MIT-SR model prediction of strain rate effects in undrained shear response of K_0-normally consolidated RBBC (after Yuan, 2016)

Figure 11 illustrates the MIT-SR predictions of strain rate effects in undrained shearing of K_0-normally consolidated RBBC. The model predicts effects of strain rate on the pre-peak stiffness ($\varepsilon_a < 0.1\%$), as well as the undrained shear strength and critical state conditions.

4. APPLICATIONS

4.1 Tunnel-Induced Ground Movements

The effects of small strain nonlinearity vary among the various classes of boundary value problems considered by Jardine et al. (1984) and Burland (1989). Perhaps the simplest class to consider are far field deformations associated with tunnelling in clay.

There are a number of very well-instrumented tunnelling projects in London clay including two cases where ground movements were measured in greenfield conditions: i) open-face shield construction of twin 4.85 m tunnels for the Jubilee Line Extension (JLE) in St James's Park (Nyren, 1998); and ii) closed-face EPB construction of twin 6.8m diameter Crossrail tunnels at sections in Hyde Park (C300; Wan et al. 2017; Ieronymaki et al. 2018).

For the JLE project, Nyren (1998) installed an array of 24 surface monitoring points (SMP; surveyed by total stations), while subsurface ground movements were recorded using a set of: 1) 9 electrolevel inclinometers, with tilt angles typically measured at vertical intervals of 2.5 m; and 2) 11 rod extensometers, each measuring vertical displacement components at up to 8 elevations.

Ground movements were measured approximately 1 day after passage of the first tunnel bore (WB), when it can reasonably be assumed that there is little consolidation within the low permeability London clay.

Standing and Burland (2006) fitted the measured transversal surface settlement trough using the empirical Gaussian relation (Peck, 1969) with a trough width, x_i = 13.3 m and maximum settlement above the crown, $u_y^0 \approx 20$ mm. Hence, the volume loss at the ground surface, ΔV_s (= $2.5 u_y^0 x_i$) corresponds to an apparent ground loss at the tunnel cavity, $\Delta V_L/V_0$ = 3.3%, caused by tunnel construction. They attribute this unexpectedly high volume loss to details of the construction method (the WB tunnel was constructed with up to 1.9 m of unsupported heading) and to a local ground zone above the WB tunnel crown with a higher concentration of sand and silt partings in the London Clay.

Extensometer measurements (Nyren, 1998) directly above the centerline of the WB tunnel show measure axial strains in the range 0.01 – 0.1% (corresponding to conditions in undrained plane strain extension) and therefore we should expect effects of anisotropic stiffness and small strain non-linearity to affect the magnitude and distribution of ground movements.

3D finite-element analysis results, after Wongsaroj (2005)

Line	Model	K_0	G_{hh}/G_{vh}	$\Delta V_L/V_0$: %	n	m
– – –	Isotropic	1·5	1·0	6·0	1·000	0·435
———	Anisotropic	1·5	1·5	5·6	0·438	0·130
– · – · –	Anisotropic	1·0	1·5	5·4	0·438	0·130
——+——+——	Anisotropic	1·2	5·0	3·2	0·438	0·039
●	Field measurements				$\left(n = \frac{v'_{vh}}{v'_{hv}}\right)$	$\left(m = \frac{n}{2(1+v'_{hh})} \frac{G_{vh}}{G_{hh}}\right)$

Poisson's ratios: isotropic ($v'_{vh} = v'_{hh} = v'_{hv} = 0{\cdot}15$);
anisotropic model ($v'_{vh} = 0{\cdot}07$, $v'_{hh} = 0{\cdot}12$, $v'_{hv} = 0{\cdot}16$)

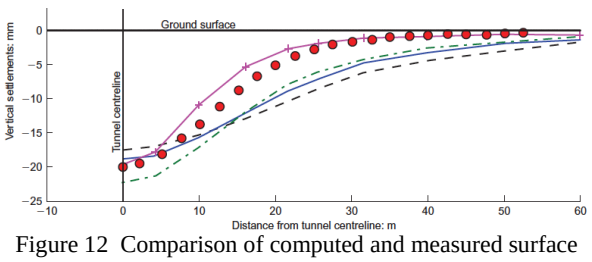

Figure 12 Comparison of computed and measured surface settlements for JLE WB tunnel construction in St James's Park using model of Wongsaroj (Zymnis et al. 2013)

Several researchers have attempted to compute the ground movements of using non-linear finite element methods (2D and 3D;

Franzius et al. 2005; Wongsaroj, 2005) using a range of constitutive models. For example, Wongsaroj (2005) formulated a bespoke constitutive model to describe the non-linear, anisotropic behavior of London clay. Figure 12 compares the measured surface settlements with computed results using four different input parameter sets. Models with both isotropic and anisotropic small strain stiffness and K_0 = 1.5 (note the properties are not consistent with values reported in later work, cf. Figure 4) resulted in settlement troughs that are wider than the field measurements for the WB JLE tunnel and also overestimate significantly the back-figured volume loss ($\Delta V_L/V_0$ = 5.4% to 6.0%). Good agreement is only achieved by increasing the anisotropic stiffness ratio (G_{hh}/G_{vh} = 5 corresponding to m = 0.04) and reducing the assumed value of K_0 = 1.2. Franzius et al. (2005) experienced similar problems and only matched the surface settlements using a very high value of n (= E'_h/E'_v = 6.25 vs 2.0 shown in Figure 4).

There are various possible causes for these discrepancies including limitations in the constitutive models (and input parameters) and difficulties in representing the boundary conditions associated with open-face tunnel construction. Given the complexity of the near field interactions between tunnel excavation, support and lining systems and the surrounding ground, Whittle and Sagaseta (2003) proposed using simplified analytical solutions for describing far-field ground deformations. Pinto and Whittle (2014) presented solutions for ground deformations (in the 2D transversal plane half-space) for two basic modes of deformation corresponding to uniform convergence and ovalization at the wall of a circular tunnel cavity, based on the assumption of linear, isotropic elastic soil behavior (u_ε, u_δ; Figure 13). Their analyses show that deformation fields based on the superposition of fundamental, singularity solutions differ only slightly from analyses that consider the physical dimensions of the tunnel cavity. Zymnis et al. (2013) extended these solutions for the case of cross-anisotropic elastic soils. For linear elastic ground properties, the distributions of ground movements are not dependent on the magnitude of the soil stiffness by do depend on stiffness ratios for cross-anisotropy (m, n; Figure 4).

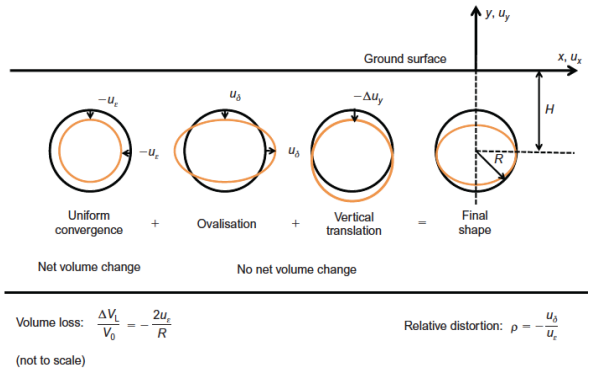

Figure 13 Cavity deformation modes used for analysis of far-field deformations caused by tunnel construction (after Whittle and Sagaseta, 2003) Note: Δu_y is a dependent parameter in half-space analytical solutions (Pinto and Whittle, 2014)

The analytic solutions have been applied to reinterpret ground deformations for the JLE WB tunnel: The cavity deformation mode parameters are evaluated using a least-squares fit to the measured surface and subsurface deformations. Figure 14 shows that both isotropic and cross-anisotropic analytical solutions achieve very good agreement with the measured vertical and horizontal ground displacements. These solutions produce very similar optimal ground loss ($\Delta V_L/V_0$) and cavity convergence parameters (u_ε) but do differ in the ovalization ratio (ρ = -u_δ/u_ε; Figure 14). The results suggest that effects of small strain anisotropy in soil stiffness have only a secondary role in the prediction of far-field ground movements.

The results in Figure 14 do not consider the nonlinearity of soil stiffness and how this might affect the distribution of ground movements. Ieronymaki et al. (2018) have investigated the performance of different tunnel construction methods using a similar method of back-analysis with optimized cavity deformation parameters. In this case, the undrained shear properties of the London clay are represented by the MIT-S1, using equivalent (self-consistent) isotropic elastic stiffness parameters in a 2D finite element model (Ieronymaki and Whittle, 2020). Figure 15 shows that the model provide a reasonable approximation of non-linear stiffness parameters measured on block samples of London clay from T5 (Gasparre, 2005).

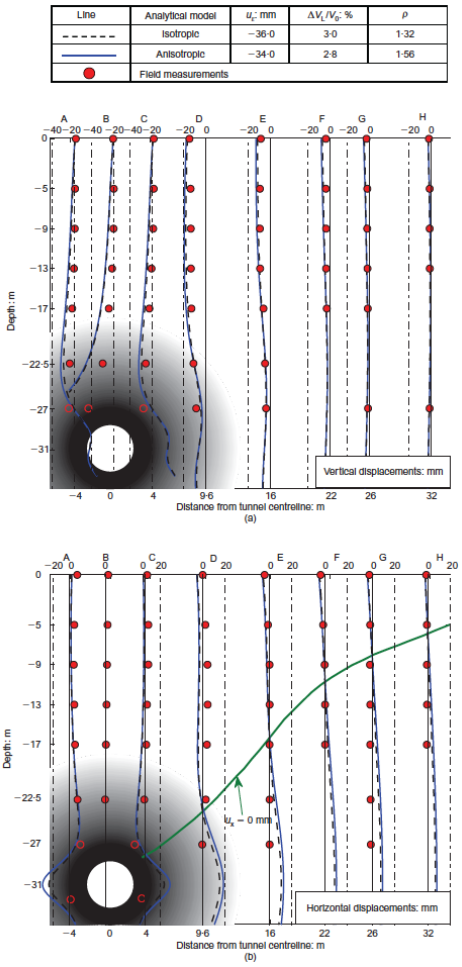

Figure 14 Comparison of analytical solutions for isotropic and cross-anisotropic elastic soils with measured data for the JLE WB tunnel in London clay using optimized cavity deformation parameters (Zymnis et al. 2013) Note: shading indicates zone of expected yield around the tunnel that could limit expected accuracy of analytical solutions

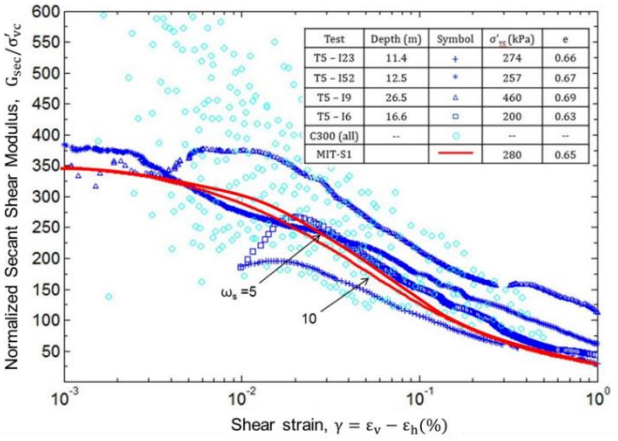

Figure 15 Non-linear stiffness of London clay simulated using MIT-S1 model with equivalent isotropic elastic parameters (Ieonymaki and Whittle, 2020)

The analyses explicitly include the depth of the clay layer and the physical dimensions of the tunnel cavity, while the surface soil units (top 7-8 m in each case) are modeled using a linear elastic soil model. Figure 16 compares the optimized solutions for the closed-face (EPB Crossrail) and open-face (JLE) methods of tunnel construction for the numerical (MIT-S1) model and analytical solutions (isotropic elastic half-space). In this case, effects of soil non-linearity should be expected to influence the cavity deformation parameters.

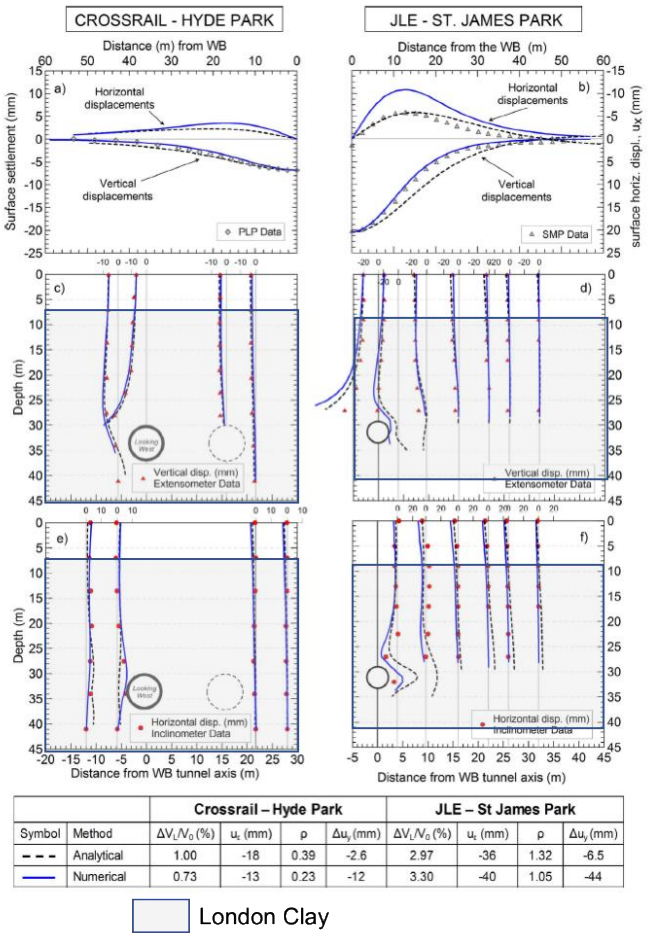

		Crossrail – Hyde Park				JLE – St James Park			
Symbol	Method	$\Delta V_L/V_0$ (%)	u_z (mm)	ρ	Δu_y (mm)	$\Delta V_L/V_0$ (%)	u_z (mm)	ρ	Δu_y (mm)
- - -	Analytical	1.00	-18	0.39	-2.6	2.97	-36	1.32	-6.5
———	Numerical	0.73	-13	0.23	-12	3.30	-40	1.05	-44

London Clay

Figure 16 Effect of soil non-linearity on far-field deformations for two tunnel projects (Ieronymaki et al. 2018)

The numerical model (i.e., FE analyses with MIT-S1) certainly achieves very good agreement with the surface settlements and subsurface measurements (sources of discrepancy in surface lateral movements for JLE are related to the modeling of the surficial soil layers) with volume losses in the range $\Delta V_L/V_0 = 0.73 – 1.00$ for the closed face EPB tunnel (Crossrail) and 2.97-3.30 for open-face tunnel construction.

Although the numerical solutions provide a much more credible representation of the elemental soil behavior, it is clear that the analytical solutions succeed in describing quite well the far-field displacements and require no site-specific calibration of material behavior. In this type of boundary value problem, it appears that linear elastic solutions can be applied successfully.

4.2 Braced Excavations

Predictions of structural response (wall deflections and bending, strut loads etc) and ground deformations are clearly important in the design of excavation support systems, especially when construction is carried out in close proximity to existing structures. Burland and Hancock (1977) conducted 2D FE analyses of the top-down construction of an underground parking garage (next to the House of Commons and Big Ben clock tower in London) assuming depth-varying linear elastic properties in the soil profile. They found significant discrepancies between predicted and measured ground surface settlements. Jardine et al. (1984) illustrated the effects of small-strain non-linearity on the excavation performance for an idealized propped retaining wall (single rigid support at the surface). They showed that soil non-linearity affected the progression of wall deflection with excavation depth but had little influence on the mode shape of the wall (at a given depth), while non-linearity affected significantly the mode shape of the surface settlements.

The construction of the Central Artery Third Harbour Tunnel (CA/T) project in Boston (1991-2007) motivated similar studies at MIT. Our interest focused on excavations occurring within deep layers of Boston Blue Clay (in some locations more than 50 m deep) where the retaining wall did not extend into a bearing layer (and ground improvement would also be prohibitively expensive). Figure 17 illustrates results of typical simulations for undrained excavation support by a 40 m deep concrete diaphragm wall with rigid props (spaced vertically at 2.5 m) within an idealized soil profile (deep layer of K_0-normally consolidated BBC). The figure compares wall deflections and surface settlements for MIT-E3 and MCC soil models (both based on prior calibration with lab data). The results at an excavation depth H = 5 m are affected by details of the initial cantilever deformation (first phase of excavation), while results at H = 20 m reflect the accumulation of ground deformations occurring below the excavated grade. While there are large differences between the magnitudes of the wall deflections predicted by the two models, the mode shapes are very similar (both predict maximum wall deflection occurring 7 m below the base of the excavation at H = 20 m). Differences in the magnitude at H = 5 m reflect the elastic stiffness properties of MCC (governed by the unloading stiffness, κ; Table 1) and MIT-E3 (which includes small strain non-linearity, conditioned by elastic stiffness, G_0). The figure also includes results from a poro-elastic model that matches the elastic stiffness properties of MCC. This shows that plasticity plays a negligible role on MCC predictions at H = 5 m (and only about 10% of the maximum wall deflection at H = 20 m). In contrast MIT-E3 is approaching failure at H = 20 m.

There are very large discrepancies between the computed surface settlements for the two soil models. Large elastic rebound in the MCC model generates upward movement of the wall and heave of the adjacent soil (assuming no slippage between wall and soil), while significant settlements extend more than 150 m behind the wall. In contrast, MIT-E3 show the development of a settlement trough with maximum deflections occurring 15-20 m behind the wall (at H = 20 m). This pattern of behaviour is more consistent with empirical data for excavations in soft-medium clays (Clough and O'Rourke, 1990).

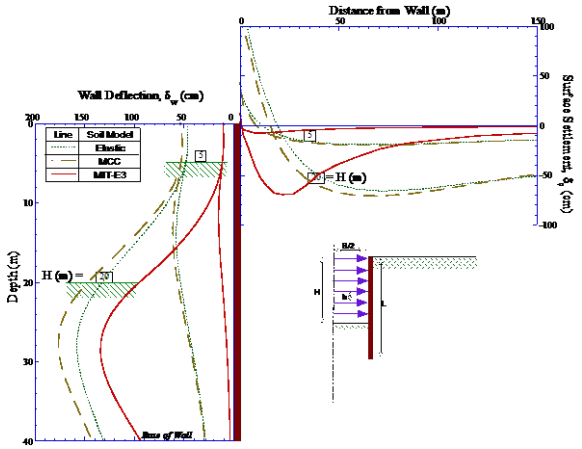

Figure 17 Numerical simulation of wall deflections and surface settlements for an idealized excavation support system in a deep layer of K_0-normally consolidated BBC (after Hashash and Whittle, 1996, 2002)

There are many factors affecting the predicted excavation performance. For example, Figure 18 shows that the settlement trough is closely linked to the depth of the clay layer while wall

deflections are linked to the onset of passive soil failure associated with large toe deflections and are unaffected by layer depth.

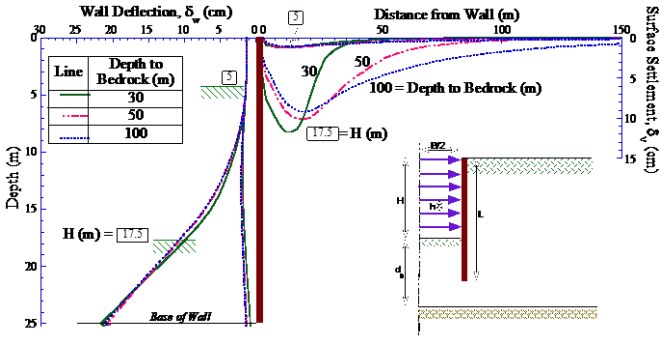

Figure 18 Effect of clay layer thickness on computed wall deflections and surface settlements using MIT-E3 soil model (25 m deep diaphragm wall in K_0-normally consolidated BBC) (Jen 1998)

The diagnosis of factors controlling the performance of excavation support systems can become quite complex. For example, Hashash and Whittle (2002) have shown that the results in the preceding figures are affected by the arching of soil against the structural supports, leading to reversals in loading directions within the clay layer as excavation progresses.

In order to evaluate the effects of small strain non-linearity it is first necessary to establish levels of shear strains that occur at different excavated grade elevations. For example, Figure 19 compares maximum shear strains, γ_{max}, throughout the soil mass for the MCC and MIT-E3 soil models at H = 10, 20, 22.5 m (depth of failure for MIT-E3). At H = 10 m, strain levels in the far-field are less than 0.1% (for MIT-E3), while near-field shearing is affected by vertical deformations of the wall and mobilization of the passive resistance below the excavated grade. At H = 20 m, γ_{max} > 0.1% from the toe of the wall up to the ground surface (more than 40m behind the wall), i.e., deep-seated movements at the toe are affecting the predictions of the trough shape shown in Figure 17. Much larger shear strains occur for MCC due to the large zone of elastic shear behaviour inside the yield surface.

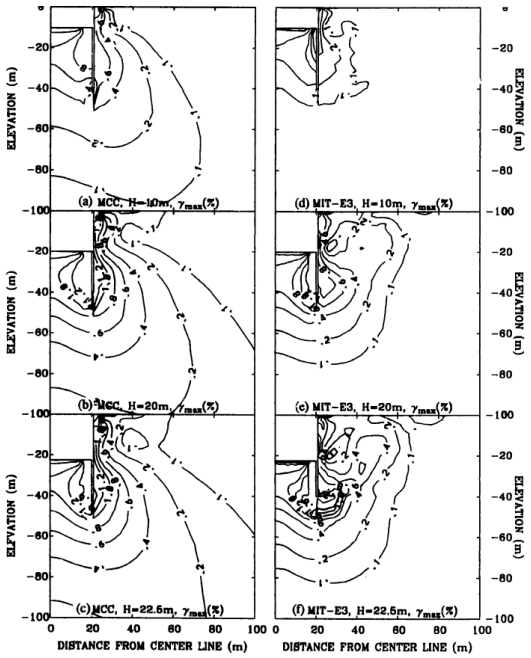

Figure 19 Computed maximum shear strain levels for deep excavation in K_0-normally consolidated BBC (Hashash, 1992)

Figure 20a compares the secant shear stiffness of the MCC and MIT-E3 soil models with laboratory measurements of plane strain, undrained shear for K_0-normally consolidated BBC. Prior papers (Whittle et al. 1994) have shown that MIT-E3 model matches closely the measured effective stress paths and undrained shear strength with the direction of the major principal stress ($s_u(\delta)$; Figure 20b). Figure 20a shows that MIT-E3 also simulates the anisotropic non-linear stiffness of BBC and can be used to map the Y1 and Y2 threshold strain surfaces (γ = 0.01, and 0.1%, respectively; cf. Figure 5) illustrated.

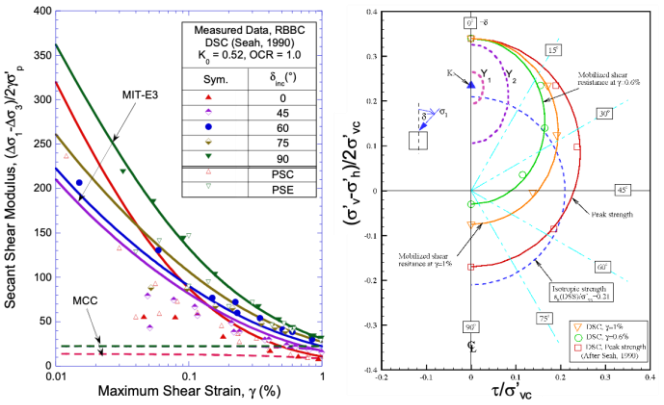

a) Effect of principal stress orientation on secant stiffness

b) MIT-E3 iso-shear strain contours for K_0-normally consolidated BBC

Figure 20 Computed and measured non-linear stiffness of K_0-normally consolidated BBC (modified from Whittle et al., 1994; Ukritchon et al. 2003)

Hashash and Whittle (2002) show that shear conditions in the retained soil involve significant rotations of principal stress directions (anticlockwise from δ = 15° to 90° during excavation; Figure 20b) and are far from undrained shear failure at H = 20 m. Hence, the settlement troughs in Figure 17 are controlled by the anisotropic, non-linear stiffness properties represented in the MIT-E3 model.

Osman and Bolton (2006) have proposed a Mobilizable Strength Design (MSD) methodology for predicted wall deflections of braced excavation support systems (for specified toe fixity conditions). Their MSD approach considers a simplified failure mechanism within the soil mass (flow beneath the base of the excavation and bending of the embedded wall section), Figure 21a. The incremental wall deformation can then be linked to an average shear strain in the soil mass (γ_{ave}) which in turn is linked to the load factor (τ/τ_f). Bolton et al. (2008) illustrate this approach using the numerical simulations for braced excavations in BBC for a range of stress history profiles (Hashash, 1992; Jen 1998), while average stress-stress properties are based on MIT-E3 simulations of undrained Direct Simple Shear (DSS) tests. These analyses achieve very reasonable predictions of wall deflections with excavation depth (Fig. 21b) but have yet to be compared with ground movements in the retained soil.

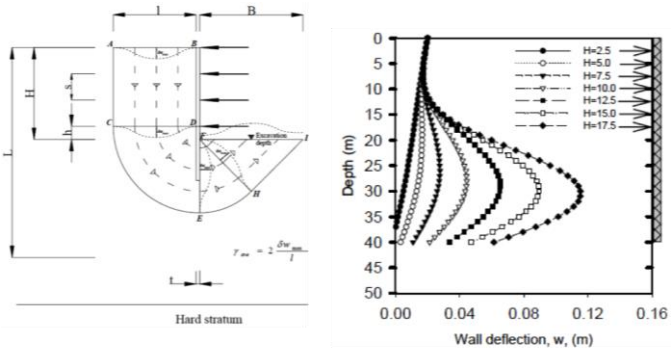

a) MSD mechanism of ground movements for braced excavation

b) MSD predictions of wall deflections in BBC (OCR = 1.0)

Figure 21 MSD design method and application for braced excavations (Osman and Bolton, 2006; Bolton, 2008)

4.3 Shallow Foundations

Burland (1989) presents several case studies to illustrate the effects of non-linear load-settlement behaviour of shallow foundations (on weathered chalk, sands and clays) that include measurements of subsurface vertical deformations. The results show very small average axial strains (< 0.1 – 0.3%) below the centreline of the foundations at working loads. Assuming that the induced stresses are largely independent of soil properties (and can be estimated from linear elastic solutions), then small strain non-linear stiffness properties cause the strains (and settlements) to concentrate much closer to the loaded area than implied by linear elasticity (consistent with analyses reported by Jardine et al. 1986). These results have had important practical implications in the refinement of empirical methods of settlement predictions based on SPT/CPT data. Burland and Burbridge (1984) use the subsurface deformation data as the basis for defining a zone of influence in their statistical interpretation of settlement data.

In fact, shallow foundations present a particularly challenging class of boundary value problem where both compression and shear properties are important, the effects of drainage conditions and stress concentrations at the edge of the footing are all related to the size of the foundation. This is a topic where generalized soil models can offer new insights. We have recently used MIT-S1 to investigate size-effects in the load-settlement response of surface foundations on deep homogeneous sand layers (Chen et al. 2020).

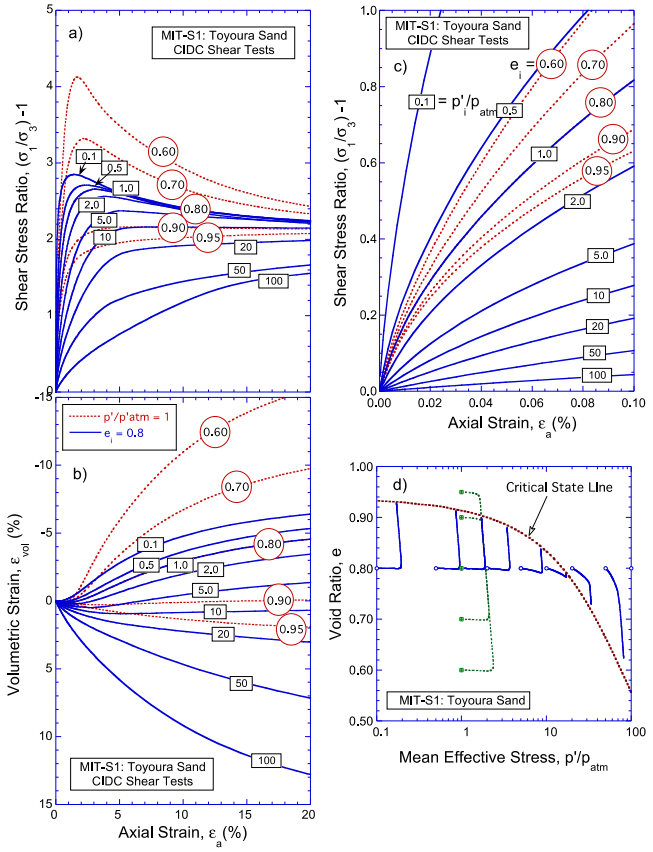

Figure 22 MIT-S1 model predictions of triaxial drained shear tests (CIDC) a) overall stress-strain, b) small-strain behaviour, c) volumetric strains, d) void ratio and critical state (adapted from Pestana et al. 2002)

Figure 22 summarizes MIT-S1 model predictions of elemental drained triaxial compression (CIDC) shear tests on Toyoura sand at a range of confining pressures (e_i = 0.8 and p'_i/p_{atm} = 0.1 – 100) and (pre-shear) void ratios (e_i = 0.6 – 0.95 at p'_i/p_{atm} = 1). These simulations generate a unique critical state condition for shearing to large axial strains (Figure 22d) that matches published data (Ishihara, 1996). The predictions show significant dilation for dense specimens and tests at low confining pressures, where peak shear resistance is mobilized at axial strain levels, 1 – 1.5% (Figures 22a, b). Figure 22c shows that there is very significant non-linearity in the predicted stress-strain response at strain levels less than 0.1%.

Figure 23a illustrates numerical simulations of the vertical load-deformation response of a 10 m diameter rough, rigid circular footing on dry sand (γ = 18 kN/m^3) using the MIT-S1 with input parameters for Toyoura sand at initial void ratios, e_0 = 0.6 – 0.9 and K_0 = 0.5, 1.0. The results are presented in a dimensionless format, showing the mobilized bearing capacity factor, $N_\gamma = 2q/\gamma' D$ for displacements up to δ/D = 20%. Results for the very dense sand (e_0 = 0.6, K_0 = 0.5) show that there is a peak foundation resistance N_γ = 72 at $\delta/D \approx$ 12%, which softens (reduces) with continued vertical deformation. In contrast, predictions for the loose and medium density cases (e_0 = 0.9, 0.8, respectively) show hardening of the foundation resistance up to large deformations. The foundation resistance increases with the assumed value of K_0. This effect is most pronounced for the very dense sand where the peak bearing capacity increases by 22% (N_γ = 88 vs 72 for K_0 = 1.0, 0.5, respectively), while the resistance at large deformations typically increases by 10-15%.

Figure 23b shows the normalized, secant foundation stiffness derived from the non-linear load-deformation response (i.e., $\overline{K} = N_\gamma D/\delta$). The secant stiffness varies inversely with the relative settlement. The highest secant stiffness occurs in the case of dense sand (e_0 = 0.6; $\overline{K}_{init}$ = 3500). The effects of small strain non-linearity are clearly seen in the degradation of $\overline{K}$ with δ_v/D. The figure compares initial foundation stiffness with $\overline{K}_{50}$ defined at 50% of peak shear resistance (i.e., at a load factor of 0.5, corresponding to δ_v/D = 2 – 4%). The results show $\overline{K}_{50}/\overline{K}_{init}$ = 0.18 – 0.40, with the largest degradation occurring for very loose sand (e_0 = 0.9).

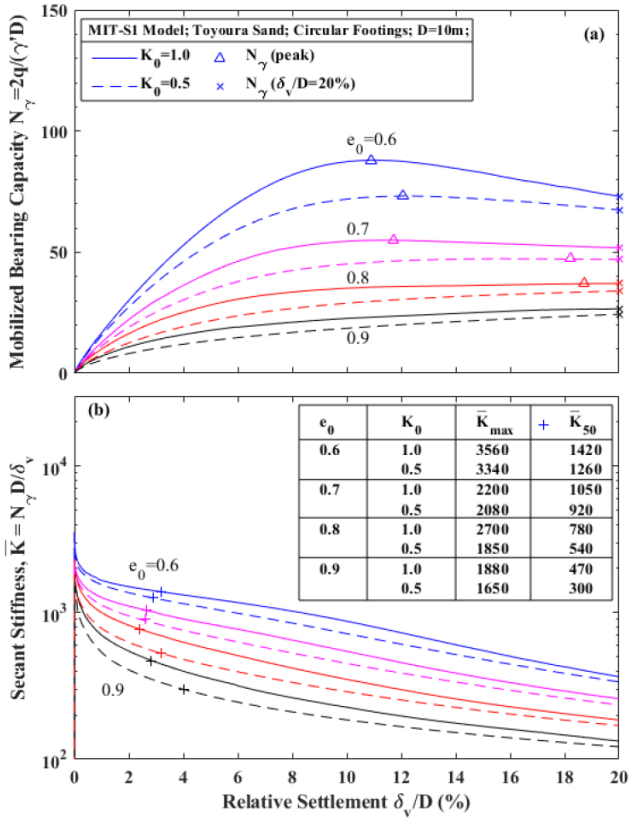

e_0	K_0	$\overline{K}_{max}$	$\overline{K}_{50}$
0.6	1.0	3560	1420
	0.5	3340	1260
0.7	1.0	2200	1050
	0.5	2080	920
0.8	1.0	2700	780
	0.5	1850	540
0.9	1.0	1880	470
	0.5	1650	300

Figure 23 Effects of void ratio on computed load-settlement response for a rigid 10 m diameter circular foundation on Toyoura sand (Chen et al. 2020)

Figure 24 summarizes the load-deformation response for a suite of analyses of circular foundations with diameters, D = 1.0 – 100 m (it should be noted that the FE mesh resolution scales with the foundation size) for deep homogeneous layers of Toyoura sand (with

K_0 = 1.0) at void ratios, e_0 = 0.6 – 0.9. The results show a large reduction in the mobilized bearing factor, N_γ, and in the normalized secant stiffness, $\overline{K}$, with foundation diameter. Peak resistance conditions are observed only for relatively small foundations on dense or very dense sand ($D \leq 10$ m for $e_0 \leq 0.7$; Figures 14a, b).

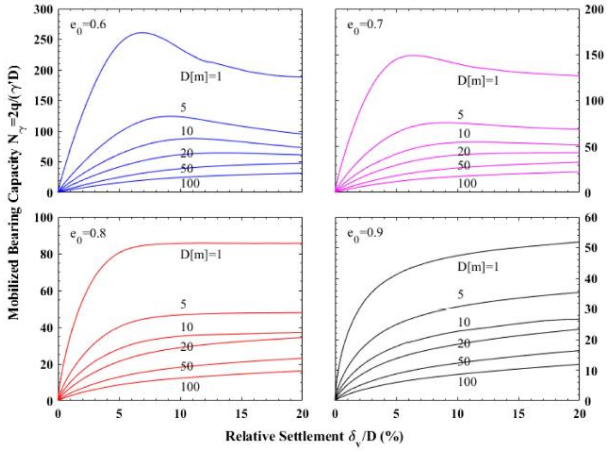

Figure 24 Predicted effects of footing diameter and sand void ratio on the normalized load-deformation response of circular foundations on Toyoura sand (Chen et al. 2020)

These results reflect changes in the deformation mechanisms with foundation size. Figures 25a-d compare the predicted deformation vector fields and contours of net volumetric strain at large deformation conditions (δ_v/D = 20%) for dense Toyoura sand (e_0 = 0.6) at D = 5, 10, 20 and 50 m. The results for smaller foundations (D = 5, 10 m; Figures 25a,b) show a large zone of net soil dilation ($\varepsilon_{vol} \geq$ 10%) extending laterally from the edge of the footing to a radius r/D = 1.0 – 1.5 and vertically to z/D = 0.5. This behavior is similar to the 'passive shear zone' for general shear mechanisms reported for rigid, plastic soil. In contrast, MIT-S1 predicts compression in the 'active zone' immediately below the foundation due to large increases in mean stress level. For larger diameter foundations (D = 20, 50 m; Figures 25c, d) the sand is compressed directly beneath the footing (i.e., zone of net soil dilation only occurs outside the foundation footprint) and there is less lateral spreading within the soil mass.

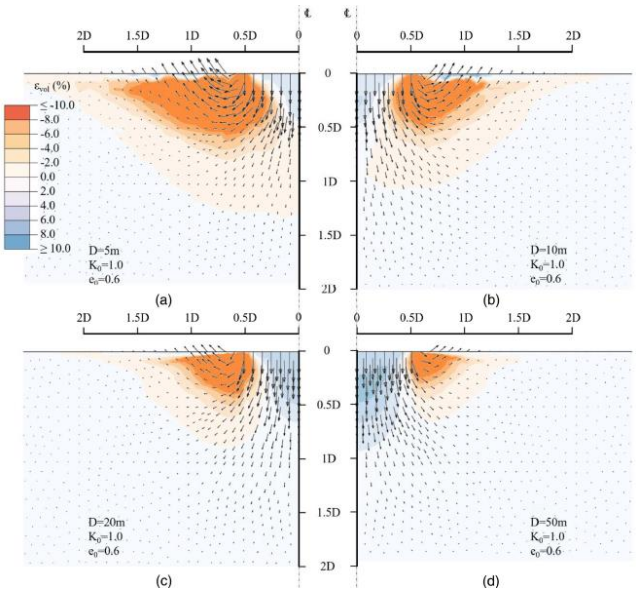

Figure 25 Effect of foundation diameter on computed deformations and volumetric strains for circular foundations on Toyoura sand at δ_v/D = 20%

The preceding results illustrate how the generalized soil model (MIT-S1) captures important scale effects affecting the performance of surface foundations on sand. Deformation fields below and adjacent to the foundations are strongly affected by plastic yielding of the sand in compression and shearing make it very difficult to isolate the effects of small-strain nonlinearity.

Burland et al. (1977) compiled a useful database of field measurements that illustrate the effects of foundation width, B, and relative density, D_r, on the coefficient of subgrade compressibility (δ_v/q). These data have subsequently been used in the development of a widely used empirical design method for predicting settlements on sand (Burland and Burbidge, 1984). Although the scatter in the data reflects variable site conditions, foundation geometry etc., it is instructive to compare directly with results of numerical analyses using MIT-S1. Figure 26 compares the computed subgrade compressibility for circular footings on Toyoura and Berlin sand at 50% of maximum bearing resistance (i.e., $\overline{K}_{50}$; Figure 23b). Subgrade compressibility increases with foundation diameter (or width). The computed results are in good agreement with the measured data. For a given foundation size, the subgrade compressibility varies over a relatively small range for dense sand, while behavior of loose sand (with much higher compressibility) is also influenced by sand type. The model captures very well the reported trends for three bands of relative density reported by Burland et al. (1977) and provide some initial validation of the predicted scale effects.

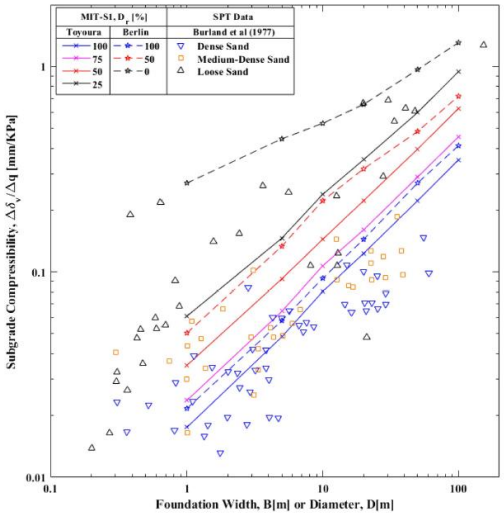

Figure 26 Comparisons of computed subgrade compressibility (load factor 0.5) with empirical data from a wide range of foundations on sand at working loads (Chen et al. 2020)

5. CONCLUSIONS

The original studies of small strain non-linearity were motivated by careful observations of field performance and enabled by advances in field and laboratory instrumentation. Laboratory measurements have resolved a long-standing discrepancy between observations of elastic stiffness from shear wave propagation and static stiffness data from laboratory element tests. The original work done by Burland and his colleagues motivated more than 30 years of research to understand and model small strain non-linearity properties of soils. The resulting data has had a major impact in the development of constitutive models that can represent this behaviour and their application (primarily through finite element analyses) for practical problems.

Over the last 30 years, finite element analyses have become ubiquitous within geotechnical practice, due in part, to the availability of robust commercial software (and of course, the massive increase in computational power). Predictions of field performance are often dependent on the soil models and availability of data for estimating model input parameters. The development and widespread usage of models such as HSS (Benz, 2007) illustrates the importance of small-strain non-linearity within these programs.

The complexity of soil properties makes the development of generalized soil models particularly challenging. This paper has

shown how more comprehensive formulations (such as MIT-E3 and MIT-S1) can be used to provide insights to explain how soil properties affect performance for different classes of boundary value problem. Taking a cue from the studies done by Burland and his colleagues, the current paper show how simplified linear elasticity may be suitable for tunnel-induced, far-field ground deformations, while non-linear stiffness properties are essential for wall deflections and ground movements around braced excavations. A generalized soil model has proved indispensable for understanding scale effects of shallow foundations on sand.

6. ACKNOWLEDGMENTS

I would like to thank the organizers of the SEAGS special volume for extending an invitation to write this paper. The shutdown of normal academic research activities due to the coronavirus epidemic has provided an unusual opportunity for introspection and reflection on this topic (which dates back to the start of my own research career).
I am very grateful to acknowledge the inspiration provided by John Burland.
I would also especially like to thank my colleagues, current and former students whose work I have extensively cited in this paper including Dominic Asimaki, Jialiang Chen, Youssef Hashash, Eva Ieronymaki, Lucy Jen, Juan Pestana, Federico Pinto, Boonchai Ukritchon, Yixing Yuan and Despina Zymnis.

7. REFERENCES

Assimaki, D., Kausel, E. and Whittle, A. J. (2000) "A model for the dynamic shear modulus and damping of granular soils," *ASCE Journal of Geotechnical & Geoenvironmental Engineering*, 126(10), pp. 859-870.

Bellotti, R., Jamiolkowski, M., Lo Presti, D. C. F. and O'Neill, D. A. (1996) "Anisotropy of small strain stiffness in Ticino sand," *Géotechnique*, 46(1), pp. 115-131.

Benz, T. (2007) "Small-strain stiffness of soils and its numerical consequences," Ph.D Thesis, U. Stuttgart.

Bobko, C. P. (2008) "Assessing the mechanical microstructure of shale by nanoindentation: The link between mineral composition and mechanical properties," Ph.D Thesis, Massachusetts Institute of Technology.

Bolton, M. D. (2008) "Supporting excavations in clays – form analysis to decision making," *Proc. 6th Intl. Conf. on Geotechnical Aspects of Underground Excavation in Soft Ground*, IS' Shanghai, 15-28

Burland, J. B. (1989) "Ninth Laurits Bjerrum Lecture: 'Small is beautiful' – The stiffness of soils at small strains," *Canadian Geotechnical Journal*, 26, pp. 499-516.

Burland, J. B. and Hancock, R. J. R. (1977) "Underground car park at the House of Commons, London, geotechnical aspects," *Structural Engineer*, 55, pp. 87-100.

Burland, J. B. & Symes, M. J. P. R. (1982) "A simple axial displacement gauge for use in the triaxial apparatus," *Géotechnique*, 32, pp. 62-65.

Burland, J. B., and Burbridge, M. C. (1984) "Settlement of foundations on sand and gravel," *Glasgow and West of Scotland Association Centenary Lecture.*

Burland, J. B., Broms, B. B. & DeMello, V. F. B. (1977) "Behavior of foundations and structures," State of the Art Report, *Proc. 9th Int. Conf. Soil Mechanics & Foundation Engineering, Tokyo*, 2: pp. 495-546.

Chen, J., Dong, Y. and Whittle, A. J. (2020) "Prediction and evaluation of size effects for surface footings on sand," *ASCE Journal of Geotechnical & Geoenvironmental Engineering*, 146(5), 0402022, DOI: 10.1061/(ASCE)GT.1943-5606.0002237

Clayton, C. R. I. (2011) "Stiffness at small strain," *Géotechnique*, 61(1), pp. 5-37.

Clough, G. W. and O'Rourke, T. D. (1990). "Construction induced movements of insitu Walls." *Design and Performance of Earth Retaining Structures,* ASCE GSP No. 25, pp. 439-470.

Cuccovillo, T. & Coop, M. R. (1997) "The measurement of local axial strains in triaxial tests using LVDTs," *Géotechnique*, 47(1), pp. 167-171.

Dafalias, Y. and Herrmann, G. R. (1982) "Bounding Surface Formulation of Soil Plasticity," Chapter 10 in *Soil Mechanics, Transient and Cyclic Loads*, eds. G.N. Pande & O.C. Zienkiewicz, Wiley and Sons.

Di Benedetto, H., Tatsuoka, F. and Ishihara, M. (2002) "Time-dependent shear deformation characteristics of sand and their constitutive modelling," *Soils & Foundations*, 42(2), pp. 1-22.

Drnevich, V. P., Hardin, B. O., & Shippy, D. J. (1978) "Modulus and damping of soils by the resonant column method," *ASTM STP 654*, pp. 91-125.

Duncan, J. M., and Chang, C. Y. (1970) "Nonlinear analysis of stress and strain in soils," *Journal of the Soil Mechanics and Foundations Division, ASCE*, 96(SM5), pp. 1629-1653.

Franzius, J. N., Potts, D. M. and Burland, J. B. (2005) "The influence of soil anisotropy and K_0 on ground surface movements resulting from tunnel excavation," *Géotechnique*, 55(3), pp. 189-199.

Gasparre, A., Nishimura, S., Minh, N. A., Coop, M. R. and Jardine, R. J. (2007) "The stiffness of natural London Clay," *Géotechnique*, 57(1), pp. 33–47

Goto, S., Tatsuoka, F., Shibuya, S., Kim, Y. S., & Sato, T. (1991) "A simple gauge for local small strain measurements in the laboratory," *Soils and Foundations*, 31(1), pp. 169-180.

Hashash, Y. M. A. and Whittle, A. J. (1996). "Ground movement prediction for deep excavations in soft clay," *ASCE Journal of Geotechnical Engineering*, 122(6), pp. 474-486.

Hashash, Y. M. A. and Whittle, A. J. (2002). "Load transfer mechanisms and arching in braced excavations in soft clay," *ASCE Journal of Geotechnical & Geoenvironmental Engineering*, 128(3), 187-197.

Hoque, E., and Tatsuoka, F. (1998) "Anisotropy in elastic deformation of granular materials," *Soils and Foundations*, 38(1), pp. 163–179.

Hueckel T. and Nova, R. (1979) "Some hysteresis effects of the behavior of geological media," *International Journal of Solids and Structures*, 15, pp. 625-642.

Ieronymaki, E., Whittle, A. J. and Einstein, H. H. (2018) "Comparative study of the effects of three tunneling methods on ground movements in stiff clay," *Tunneling and Underground Space Technology*, 74, pp. 167-177.

Ieronymaki, E., and Whittle, A. J. (2020) "Application of generalized plasticity model for representing the behavior of a highly overconsolidated clay," *submitted for publication*.

Ishihara, K. (1996) *Soil Behaviour in Earthquake Geotechnics*, Oxford University Press, Oxford.

Iwan, W. D. (1967) "On a class of models for the yielding behavior of continuous and composite systems," *Journal of Applied Mechanics, Transactions ASME*, pp. 612-617.

Jardine, R. J. (1985) "Investigations of pile-soil behaviour with special reference to the foundations of offshore structures," PhD Thesis, Imperial College, London.

Jardine, R. J., Symes, M. J. P. R. & Burland, J. B. (1984) "The measurement of soil stiffness in the triaxial apparatus," *Géotechnique*, 34(3), pp. 323-340.

Jardine, R. J., Potts, D. M., Fourie, A. B. & Burland, J. B. (1986) "Studies of the influence of non-linear stress-strain characteristics in soil-structure interaction," *Géotechnique*, 36(3), pp. 377-396.

Jardine, R. J., Kuwano, R., Zdravkovic, L., & Thornton, C. (2001) "Some fundamental aspects of the pre-failure behaviour of granular soils." In, *Pre-failure Deformation Characteristics of Geomaterials*, Balkema, Lisse, (2), pp. 1077–1112.

Jen, L. C. (1998) "The design and performance of deep excavations in clay," Ph.D Thesis, Massachusetts Institute of Technology.

Jiang, Y. M. and Liu, M. (2009) "Granular Solid Hydrodynamic," *Granular Matter*, 11(3), pp. 139-156.

Kamrin, K. and Bouchbinder, E. (2014) "Two-temperature continuum thermodynamics of deforming amorphous solids," *Journal of the Mechanics and Physics of Solids*, 73, pp. 269-288.

Kim, T. and Finno, R. (2014) "Elastic shear modulus of compressible Chicago clay," *KSCE Journal of Civil Engineering*, 18(7), pp. 1996-2006.

Mitchell, J. K. and Soga, K. (2005) *Fundamentals of Soil Behavior*, 3rd Edition, Wiley & Sons, Inc., New York.

Mróz, Z., Norris, V. A. and Zienkiewicz, O. C. (1978) "An anisotropic hardening model for soils and its application to cyclic Loading," *International Journal for Numerical and Analytical Methods in Geomechanics*, 2, pp. 203-221.

Mróz, Z., Norris, V. A. and Zienkiewicz, O. C. (1979) "Application of an anisotropic hardening model in the analysis of elasto-plastic deformation of soils," Géotechnique, 29(1), pp. 1-34.

Niemunis, A. and Herle, I. (1997) "Hypoplastic model for cohesionless soils with elastic strain range," *J. Mechanics of Cohesive & Frictional Materials*, 2(4), pp. 279-299

Nyren, R. J. (1998) "Field measurements above twin tunnels in London Clay," Ph.D Thesis, Imperial College, London.

Ortega, J. A., Ulm, F. J. and Abousleiman, Y. (2008) "The nanogranular acoustic signature of shale," *Geophysics*, 74(5), pp. D65-D84

Osman, A. S. and Bolton, M. D. (2006) "Ground movement prediction for braced excavations in undrained clay," *ASCE Journal of Geotechnical & Geoenvironmental Engineering*, 132(4), pp. 465-477.

Peck, R. B. (1969) "Deep excavations and tunnels in soft ground," *Proc. 7th International Conference on Soil Mechanics and Foundation Engineering*, pp. 225-290.

Pestana, J. M. (1994) "A unified constitutive model for clays and sands." Sc.D. Thesis, Massachusetts Institute of Technology, Cambridge, MA.

Pestana, J. M. and Whittle, A. J. (1999). "Formulation of a unified constitutive model for clays and sands", *International Journal for Numerical and Analytical Methods in Geomechanics*, 23, pp. 1215-1243.

Pinto, F. and Whittle, A. J. (2014) "Ground movements due to shallow tunnels in soft ground: 1. Analytical solutions," *ASCE Journal of Geotechnical and Geoenvironmental Engineering*, 140(4), 0401.3040.

Prévost, J. H. (1977) "Mathematical modelling of monotonic and cyclic undrained clay behavior," *International Journal for Numerical and Analytical Methods in Geomechanics*, 1, pp. 196-216.

Roscoe, K. H. & Burland, J. B. (1968) "On the generalized stress-strain behaviour of wet clay," *Proc. Symp. on Engineering Plasticity*, Cambridge University Press, pp. 535-609.

Rowe, P. W. (1962) "The stress dilatancy relation for static equilibrium of an assembly of particles in contact," *Proc Royal Society*, A269, pp. 500-527.

Santagata, M. C. (1998) "Factors affecting the initial stiffness and stiffness degradation of cohesive soils," Ph.D Thesis, Massachusetts Institute of Technology.

Santagata, M. C., Germaine, J. T., and Ladd, C. C. (2007) "Small-strain nonlinearity of normally consolidated clay," ASCE, *Journal of Geotechnical and Geoenvironmental Engineering, 133*(1), pp. 72–82.

Schanz, T., Vermeer, P. A. and Bonnier, P. G. (2000) "Formulation and verification of the Hardening-Soil model," *Beyond 2000 in Computational Geotechnics*, Balkema.

Sheahan, T. C., Germaine, J. T. & Ladd, C. C. (1990) "Automated triaxial testing of soft clays: An upgraded commercial system," *ASTM Geotechnical Testing Journal*, 13(3), pp. 153-163.

Shibuya, S., Mitachi, T., Fukuda, F., and Degoshi, T. (1995) "Strain rate effects on shear modulus and damping of normally consolidated clay," *ASTM Geotechnical Testing Journal*, 18(3), pp. 365-375.

Smith, D. W. (2001) "Granular temperature," *International Journal of Geomechanics*, 1(2), pp. 249–271.

Sorensen, K. K., Baudet, B. A. and Simpson, B. (2007) "Influence of structure on the time-dependent behaviour of a stiff sedimentary clay," *Géotechnique*, 57(1), pp. 113-124.

Standing, J. R. and Burland, J. B. (2006) "Unexpected tunnelling volume losses in the Westminster area, London," *Géotechnique*, 56(1), pp. 11-26.

Tatsuoka, F. and Shibuya, S. (1992) "Deformation characteristics of soils and rocks from field and laboratory tests." *Proc. 6th Asian Conf. Soil Mechs & Foundation Engrg.*, Bangkok, 2, pp. 101-170.

Tatsuoka, F., Sato, T., Park, C. S., Kim, Y. S., Mukabi, J. N., and Kohata, Y. (1994) "Measurements of elastic properties of geomaterials in laboratory compression tests," *ASTM Geotechnical Testing Journal*, 17(1), pp. 80-94.

Tatsuoka, F., Lo Presti, D.C.F. & Kohata, Y. (1995) "Deformation characteristics of soils and soft rocks from monotonic and cyclic loads and their relationships." *Proc. 3rd Intl. Conf. Recent Advances in Geotechnical Earthquake Engrg. & Soil Dynamics*, St Louis, 1, 851-879.

Ukritchon, B., Whittle, A. J. & Sloan, S. W. (2003). "Undrained stability of braced excavations in clay," *ASCE Journal of Geotechnical and Geoenvironmental Engineering*, 129(8), pp. 738-756.

Wan, M. S. P., Standing, J. R., Potts, D. M. and Burland, J. B. (2017) "Measured short-term ground surface response to EPBM tunneling in London Clay," *Géotechnique*, 67(5), pp. 420–445.

Whittle, A. J. (1987) "A constitutive model for overconsolidated clays with applications to the cyclic loading of friction piles," Sc.D Thesis. Massachusetts Institute of Technology.

Whittle, A. J. and Kavvadas, M. J. (1994) "Formulation of the MIT-E3 constitutive model for overconsolidated clays," *ASCE Journal of Geotechnical Engineering*, 120(1), pp. 173-199.

Whittle, A. J., DeGroot, D. J., Ladd, C. C. & Seah, T-H. (1994). "Model prediction of the anisotropic behavior of Boston Blue Clay," *ASCE Journal of Geotechnical Engineering*, 120(1), pp. 199-225.

Whittle, A.J. & Hashash, Y.M.A. (1994) "Soil modeling and prediction of deep excavation behavior," *Proc. International Symposium on Pre-Failure Deformation Characteristics of Geo-Materials*, Sapporo, 1, 589-595.

Whittle, A. J. and Sagaseta, C. (2003) "Analyzing the effects of gaining and losing ground," *Soil Behavior and Soft Ground Construction*, ASCE GSP No. 119, pp. 255-291.

Wichtmann, T., Fuentes, W. and Triantafyllidis, T. (2019) "Inspection of three sophisticated constitutive models based on monotonic and cyclic tests on fine sand: Hypoplasticity vs Sanisand vs ISA." *Soil Dynamics & Earthquake Engineering*, 124, pp. 172-183.

Wongsaroj, J. (2005) "Three-dimensional finite element analysis of short and long-term ground response to open-face tunnelling in stiff clay," Ph.D Thesis, University of Cambridge.

Yuan, Y. (2016) "A new elasto-viscoplastic model for rate-dependent behavior of clays," Ph.D Thesis, Massachusetts Institute of Technology.

Yuan, Y. and Whittle, A. J. (2020a) "Formulation of a new elastoviscoplastic model for time-dependent behavior of clay," accepted for publication *International Journal of Numerical and Analytical Methods in Geomechanics*.

Yuan, Y. and Whittle, A. J. (2020b) "Calibration and validation of a new elastoviscoplastic soil model," accepted for publication *International Journal of Numerical and Analytical Methods in Geomechanics*.

Zymnis, D. M., Chatzigiannellis, Y. and Whittle, A. J. (2013) "Effect of anisotropy in ground movements caused by tunneling," *Géotechnique*, 63(13), pp. 1083-1102.